Properties of Elliptical Galaxies

The first step in investigating the evolution of galaxies is to understand the properties of those galaxies today. We'll start with the elliptical galaxies, which are basically very old stellar populations, with little evidence of recent star formation. We can summarize their properties as follows:

• In general, elliptical galaxies, as projected on the sky, have complete 2-dimensional symmetry. The question as to whether these objects are symmetric in practice, or are tri-axial is open (though dynamical modeling suggests that triaxiality can only last for a short time). Some ellipticals have "fine structure," such as very weak ripples, shells, and boxy (not elliptical) isophotes. These signatures are weak, but real. In general, those ellipticals with fine structure are *slightly* bluer than equivalent galaxies without fine structure. Disky ellipticals also have more rotation than boxy ellipticals; the latter have very low values of v/σ.

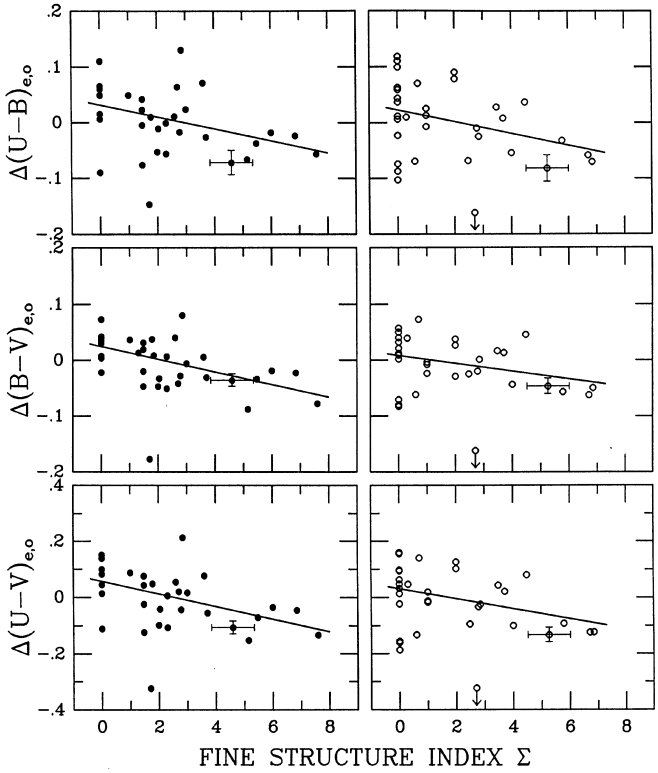

FIG. 2. Correlations between color residuals and fine-structure index Σ for 35 ellipticals (left, solid dots) and 34 S0 galaxies (right, open circles). The residuals for ellipticals were determined from least-squares fits to 227 E galaxies (see Table 2), and those for S0 galaxies from fits to 241 S0's. Solid lines mark the mean ΔC_r–Σ relations given in Table 3. Note that the color residuals, and by implication the colors themselves, get systematically bluer as Σ increases.

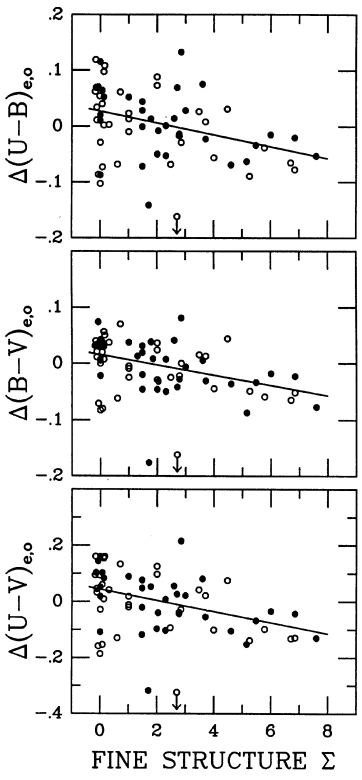

FIG. 3. Correlations between color residuals and Σ for combined sample of 69 E+S0 galaxies (E: solid dots; S0: open circles). The residuals were determined from least-squares fits to 474 E+S0 galaxies (see Table 2). To diminish point crowding at Σ=0, arbitrary shifts of up to ±0.15 in Σ have been applied to these points. Solid lines mark the mean ΔC_r–Σ relations given in Table 3.

[Schweizer & Seitzer 1992, *A.J.* **104,** 1039]

• Ellipticals range in flattening from E0 (round) to E7. No elliptical is flatter than E7. The data are *not* consistent with the hypothesis that all ellipticals are E7 and appear rounder by the effects of random viewing angles. Most likely there is a spread of flattenings centered about E3, or thereabouts. Their flattening is also inconsistent with the idea of rotational support – rotation is unimportant in most systems.

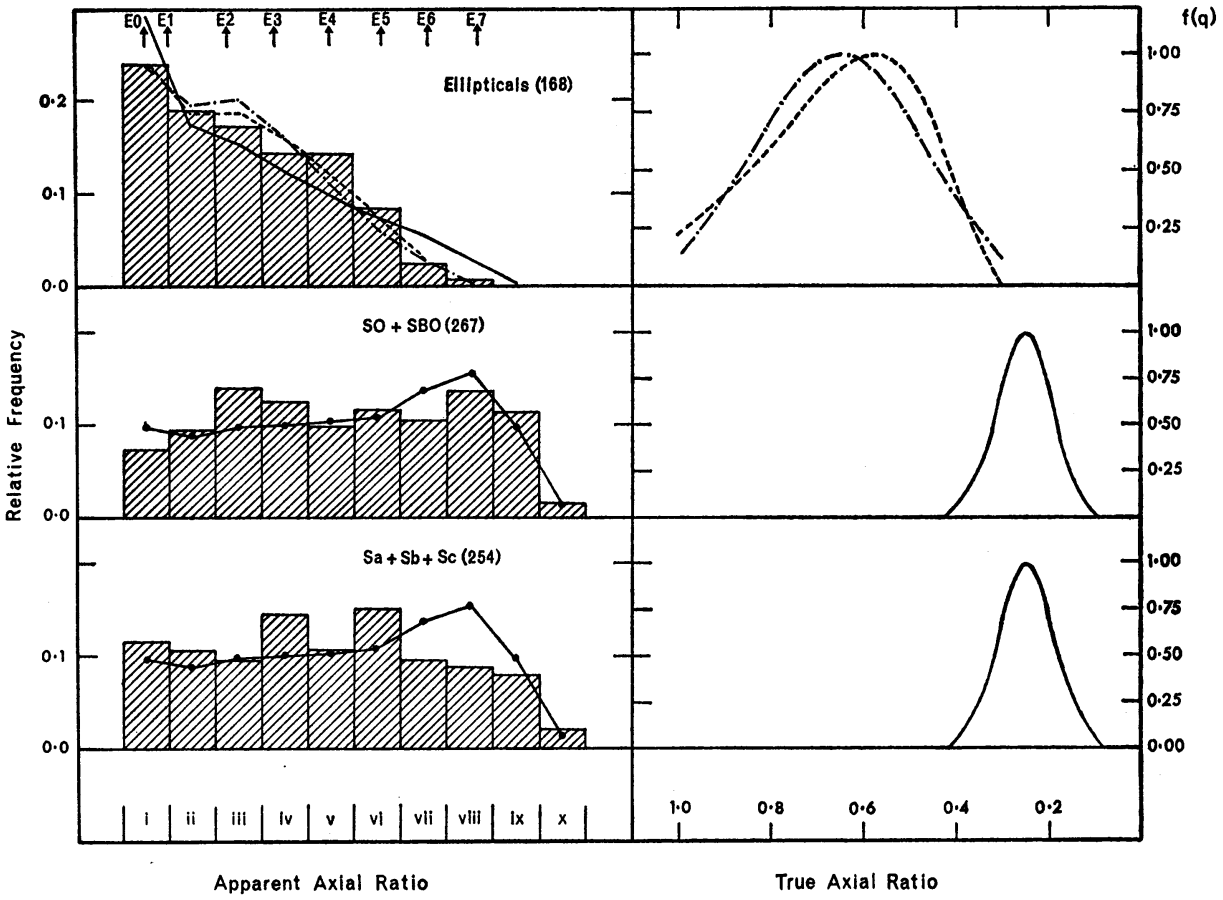

FIG. 1.—*Left*, histograms of the distribution of apparent axial ratios for E, S0, and spiral galaxies, sorted into class intervals defined in Tables 1 and 2. The curves are predicted ratios for various assumptions of the distribution of intrinsic flattening. *Right*, assumed intrinsic distributions corresponding to the curves on the left. The case of uniform flattening for E galaxies is a straight horizontal line truncated at $b/a = 0.3$ and is not shown. Dot-dash curve is a Gaussian with $q_0 = 0.65$ and $\sigma = 0.18$. Dashed curve is a skewed binomial distribution defined in the text, with $q_0 = 0.58$, $a = 0.31$, and $p = 3.0$. The two solid curves are Gaussians with $q_0 = 0.25$ and $\sigma = 0.06$.

[Sandage, Freeman, & Stokes 1970, *Ap.J.*, **160**, 831]

• There is little or no star formation in elliptical galaxies. However, the spectral energy distribution of some ellipticals turns up in the ultraviolet. (In other words, since elliptical galaxies are made up of old stars, the composite spectrum of an elliptical should look like that of a $\sim 4,000°$ K giant. However, many ellipticals are brighter at 1500 Å than they are at 2000 Å.)

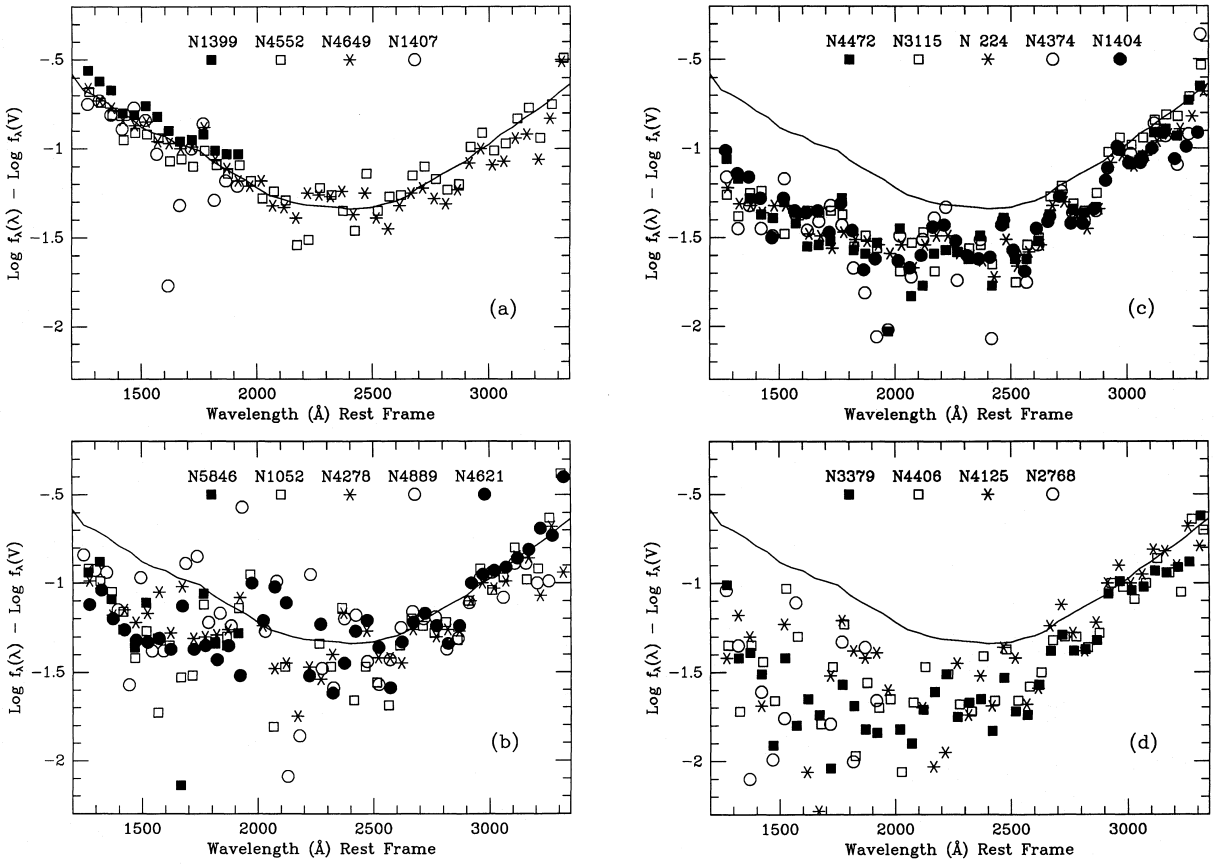

FIG. 2.—Eight panels plotting the reddening-corrected and redshift-corrected ultraviolet spectra for 27 of 32 galaxies in this sample. All spectra are plotted as $\log f_\lambda - \log f_V$ vs. wavelength and are divided according to their position in the $(1550 - V)$, Mg_2 diagram (Fig. 1*a*). (*a*) The four quiescent galaxies with the bluest $(1550 - V)$ colors. (*b*), (*c*), (*d*), and (*e*): 15 quiescent and two active galaxies, arranged in order of $(1550 - V)$. Note the high degree of similarity of the ultraviolet spectra of quiescent galaxies with similar values of $(1550 - V)$ and Mg_2. (*f*) The two bluest star-forming galaxies. (*g*) The two reddest star-forming galaxies. (*h*) The two active galaxies with the bluest $(1550 - V)$ colors; note possible excess emission from 2000 to 2500 Å with respect to blue quiescent galaxies.

[Burstein *et al.* 1988, *Ap.J.*, **328**, 440]

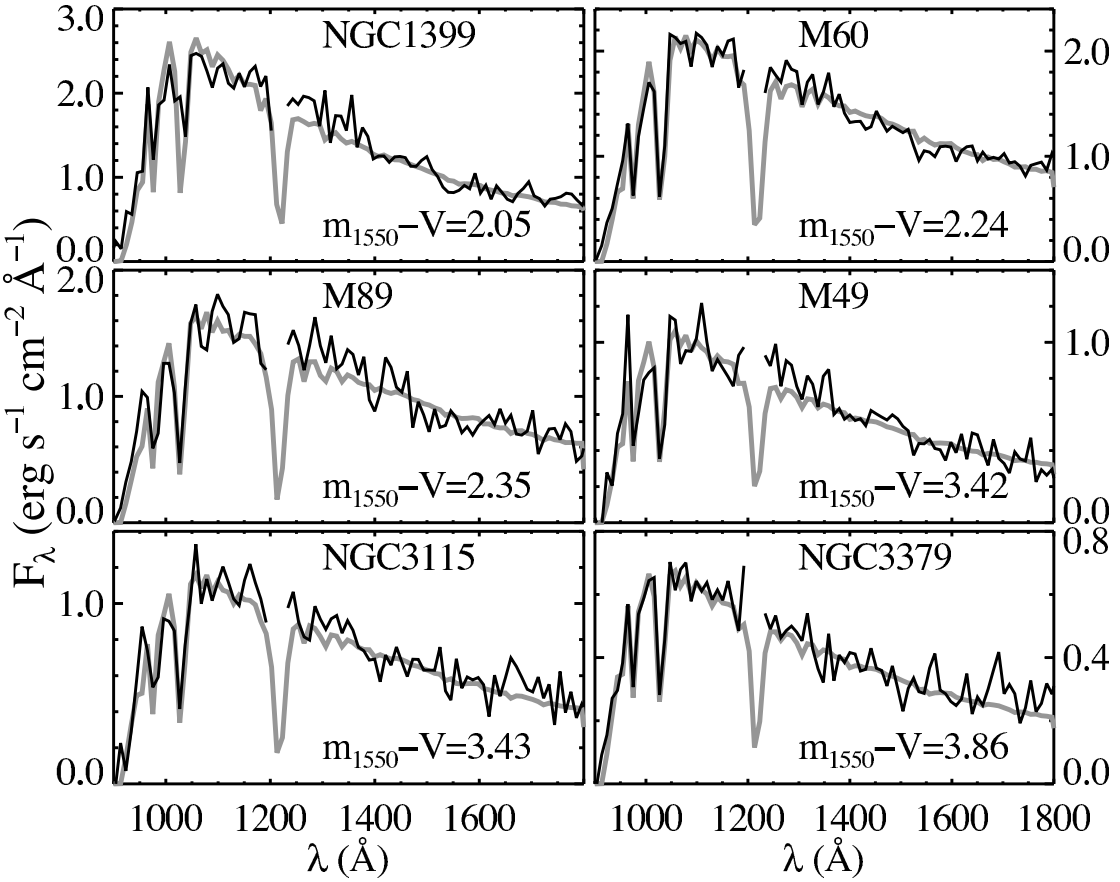

Figure 1. Spectra of six elliptical galaxies observed with the Hopkins Ultraviolet Telescope (*black curves*). Although the galaxies span a large range in $m_{1550} - V$ (labeled), they all appear very similar, and are well-matched by the integrated light (*grey curves*) of EHB stars and their progeny, spanning a narrow range of envelope mass.

[Brown 2004 *Ap. Spac. Sci.*, **291** 215]

• There is very little cold interstellar medium in elliptical galaxies. However, there is x-ray gas at a temperature of about $T \sim 10^6$ K. One can easily see where this gas comes from. The stars in an elliptical galaxy must be losing mass. If the stars are moving isotropically at $\sigma \sim 200$ km s^{-1}, then the atoms of lost material, if thermalized, will have a temperature of

$$\frac{1}{2} m_H \sigma^2 \sim \frac{3}{2} kT \Longrightarrow \ T \sim 10^6 \text{ degrees K} \qquad (6.01)$$

• Most ellipticals have weak radial color gradients: they are redder on the inside than they are on the outside. This may be due to age (older stars have a redder turn-off mass), or metallicity (metal-rich stars are intrinsically redder than their metal-poor counterparts, due to the effects of H^- opacity and the line-blanketing of metals).

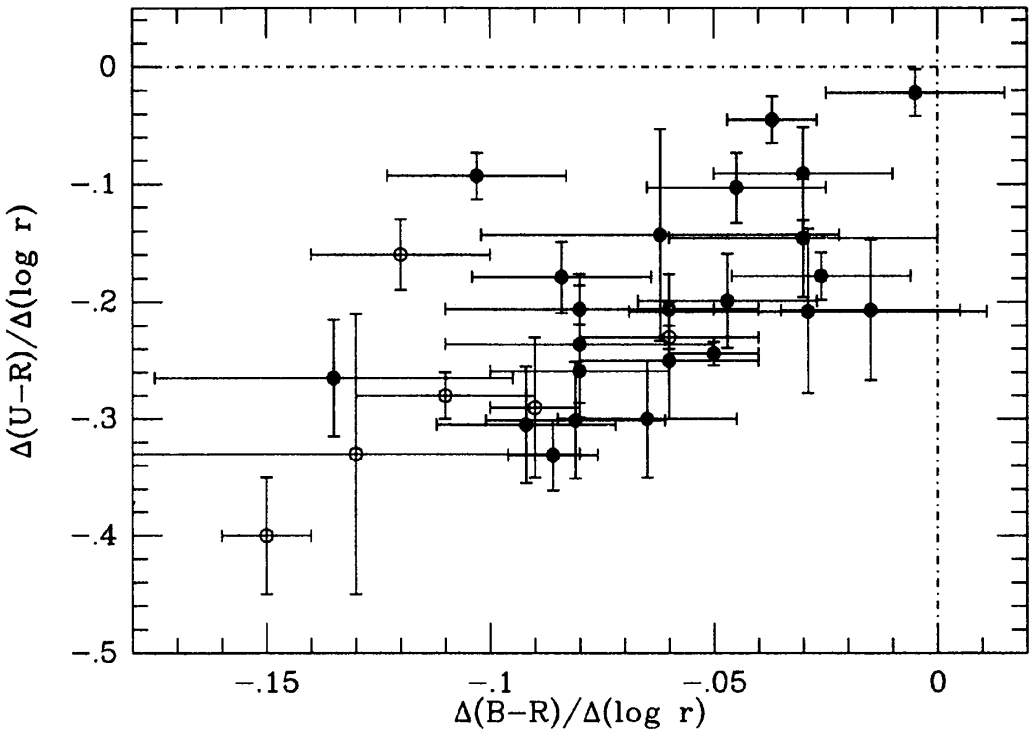

FIG. 11. Logarithmic color gradients in $U - R$ in mag dex^{-1} against color gradients in $B - R$. There is a correlation, but it is weaker than might be expected. This is mainly due to the large scatter in $\Delta(B - R)$ from observational uncertainty.

[Peletier *et al.* 1990, *A.J.*, **100,** 1091]

• There appears to be a correlation between the mass of an elliptical galaxy (or the bulge of a spiral galaxy) and its central black hole.

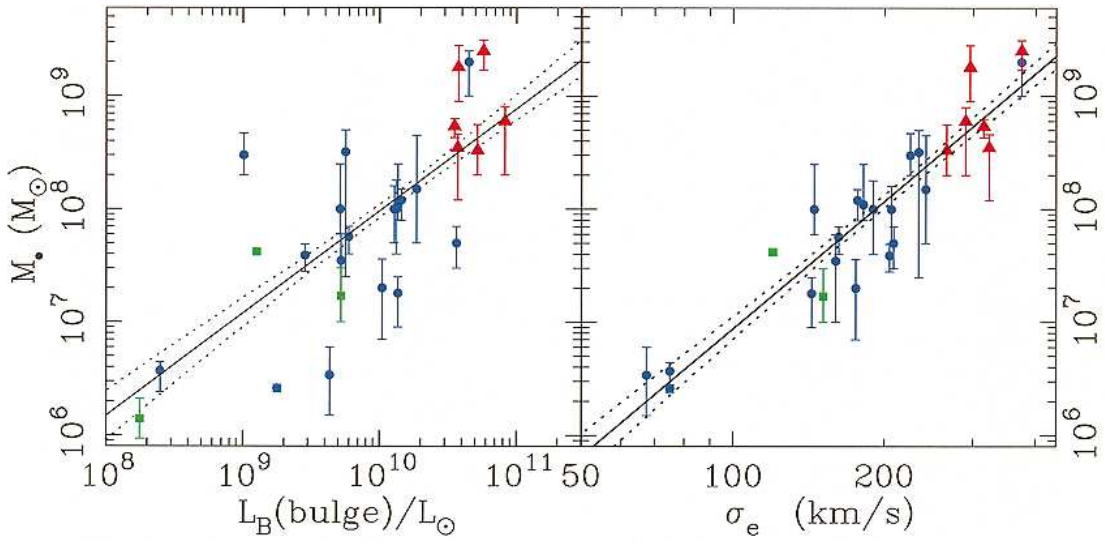

FIG. 2.—Black hole mass versus bulge luminosity (*left*) and the luminosity-weighted aperture dispersion within the effective radius (*right*). There are 26 points in the dispersion plot; 13 are new detections from stellar kinematics (K. Gebhardt et al. 2000, in preparation; G. Bower et al. 2000, in preparation). Green squares denote galaxies with maser detections, red triangles are from gas kinematics, and blue circles are from stellar kinematics. Solid and dotted lines are the best-fit correlations and their 68% confidence bands.

[Ferrarese & Merritt 2000, *Ap.J. (Letters)*, **539,** L9]
[Gebhardt, *et al.* 2000, *Ap.J. (Letters)*, **539,** L13]

The Elliptical Galaxy Fundamental Plane

Elliptical galaxies populate a "fundamental plane" in luminosity-surface brightness-velocity dispersion space. At first glance, the physics underlying this plane is easy to understand.

If you assume the stars of an elliptical galaxy are in virial equilibrium, then their typical velocity dispersion will be

$$\sigma^2 \propto \frac{\mathcal{M}}{R} \tag{6.02}$$

Now let's assume that all elliptical galaxies have the same mass-to-light ratio ($\mathcal{L} \propto \mathcal{M}$) and all have about the same surface brightness ($I = \mathcal{L}/R^2$). Then, if I is indeed a constant,

$$\sigma^2 \propto \frac{\mathcal{M}}{R} \propto \frac{\mathcal{L}}{R} \propto \frac{\mathcal{L}}{\mathcal{L}^{1/2}} \propto \mathcal{L}^{1/2} \Longrightarrow \mathcal{L} \propto \sigma^4 \tag{6.03}$$

This is called the *Faber-Jackson relation.* The velocity dispersion, σ, is usually measured near the galactic nucleus, where the galaxy is brightest (and a high signal-to-noise spectrum is obtainable).

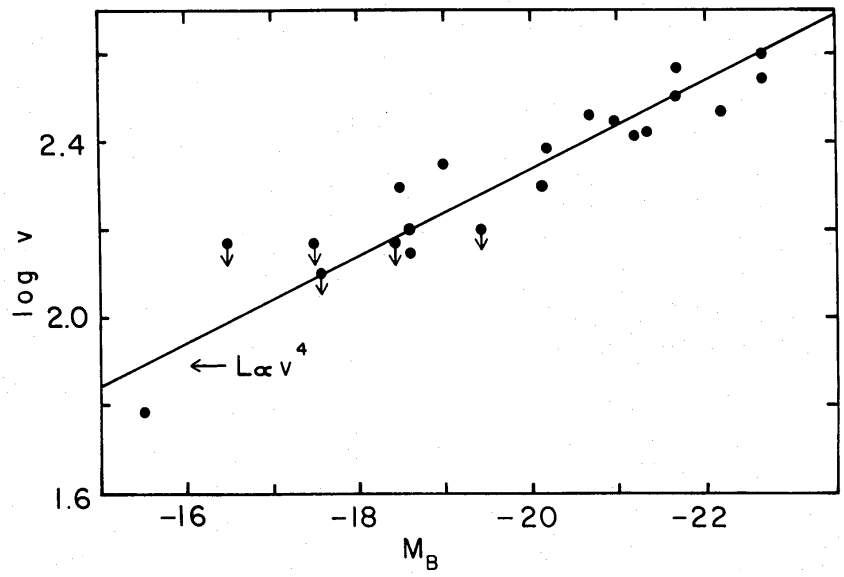

FIG. 16.—Line-of-sight velocity dispersions versus absolute magnitude from Table 1. The point with smallest velocity corresponds to M32, for which the velocity dispersion (60 km s^{-1}) was taken from Richstone and Sargent (1972).

[Faber & Jackson 1976, *Ap.J.*, **204,** 668]

Of course, all galaxies do not have the same surface brightness. So if you take $I = \mathcal{L}/R^2$ and substitute that into the virial theorem (keeping the mass-to-light ratio assumption), then a relation between luminosity, surface brightness, and velocity dispersion is the natural consequence, *i.e.,*

$$\mathcal{L} \propto \sigma^4 I^{-1} \tag{6.04}$$

Observations of real ellipticals show that when $\mathcal{L}$ is the total B-band luminosity of the galaxy, σ is the central velocity dispersion, and I is the galaxy surface brightness measured at a radius that contains 1/2 the total light from the galaxy (R_e), the exponents in (6.04) are not 4 and -1, but 2.7 and -0.7. This is the elliptical galaxy fundamental plane.

Note that (6.04) can be simplified. Dimensionally speaking, luminosity divided by surface brightness ($\mathcal{L}/I$) has the units of size squared. Thus, one group (who called themselves the Seven Samurai) combined the two variables, and took the square root, thereby creating a new characteristic size variable, D_n. (Their specific definition for D_n was that of a circular aperture that enclosed a mean blue surface brightness of 20.75 mag arcsec^{-2}, but other definitions are possible.) The best fit to the authors' (very large) dataset yielded

$$D_n \propto \sigma^{1.2} \tag{6.05}$$

Thus, the $D_n - \sigma$ relation is actually just the optimal projection of the fundamental plane into a single dimension.

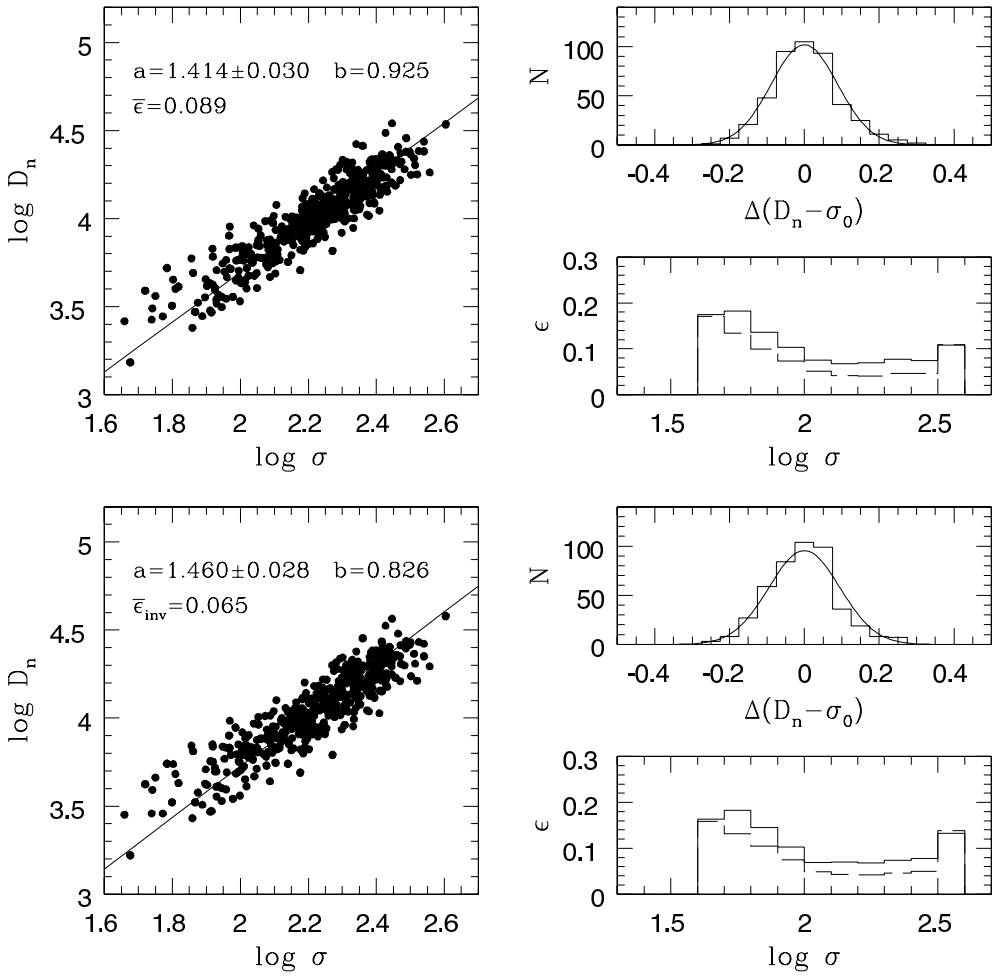

FIG. 6.—*Left panels:* filled circles show the bias-corrected measurements; straight lines show the derived bivariate distance relation (*upper panel*) and the inverse relation (*lower panel*). The values of the slope (*a*), zero point (*b*), and mean rms scatter ($\bar{\epsilon}$) are also shown. *Right panels:* Distribution of residuals relative to the D_n-σ relation, together with the distribution of the corresponding observed scatter (*solid line*) and intrinsic scatter (*dashed line*), as a function of σ.

[Dressler *et al.* 1987, *Ap. J.*, **313,** 42]
[Bernardi *et al.* 2002, *A.J.*, **123,** 2159]

Because velocity dispersion is independent of distance, but size is not, the D_n-σ (or fundamental plane) relation is a distance indicator. (You use σ to predict size, and then compare linear size to angular size.) In fact, the relation is perhaps best known for its use in measuring large-scale departures from the Hubble Flow. It is, however, among the least accurate of the (well quantified) standard candles: its scatter is $\sim 20\%$ or more. In part, this may be due to the technique's reliance on the galaxy's central velocity dispersion, which may be affected by local conditions. Fortunately, since elliptical galaxies are found in clusters, one can improve the distance estimates by analyzing multiple galaxies, and beating down the error by $\sqrt{N}$.

Interestingly, the fundamental plane is not just a relation between luminosity, size, and velocity dispersion. The relationship is reflected in many other variables. For example,

• Elliptical galaxy luminosity correlates with color. Large ellipticals are redder than small ellipticals.

• Elliptical galaxy luminosities (or velocity dispersions) correlate with absorption line strength. Bright, redder galaxies have stronger absorption features.

• Elliptical galaxy absorption features correlate with the UV upturn. Galaxies with strong absorption features have larger UV excesses.

• Elliptical galaxy UV excess correlates with the number of planetary nebulae in the galaxy. Galaxies with large UV excesses have fewer planetary nebulae (per unit luminosity).

Any of the above variables can be substituted in for the others to form a tight correlation of properties. The existence of the fundamental plane argues strongly that elliptical galaxies, as a class, are very homogeneous in their properties.

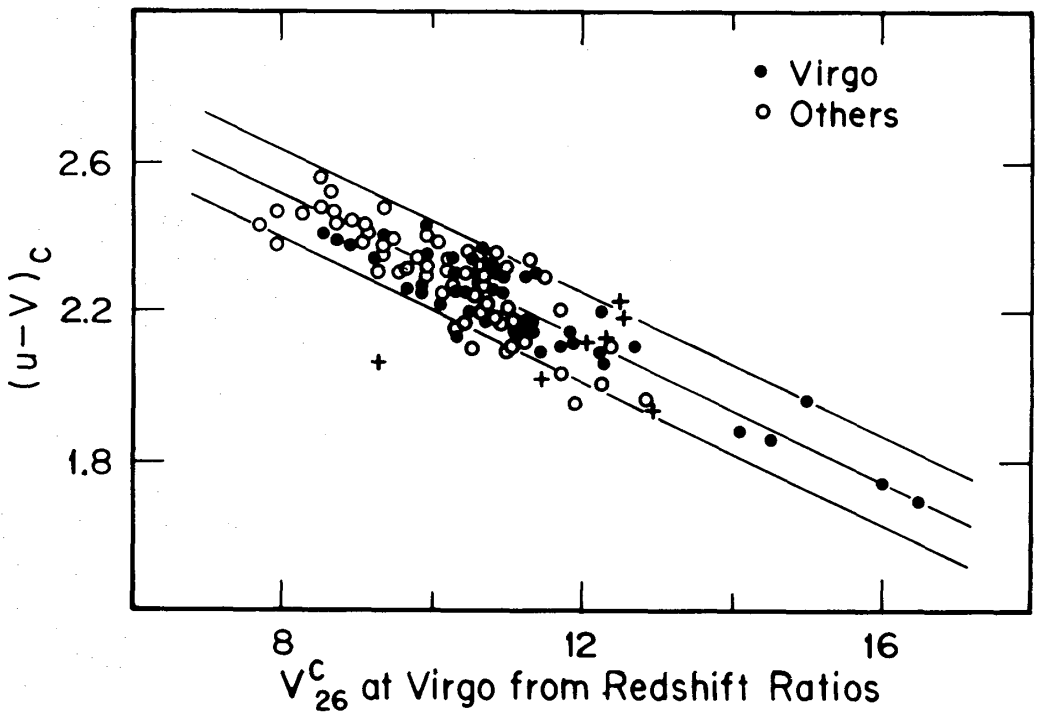

FIG. 5.—Composite C-M diagram in $(u - V)_c$ for data in Tables 3–5, brought to the Virgo cluster distance by magnitude differences related to the ratio of the redshifts. Coding separates Virgo cluster galaxies from galaxies in all other groups and clusters. *Vertical crosses*, Virgo galaxies not used in the solution. The lines are the same as in Fig. 3.

[Visvanathan & Sandage 1977, *Ap.J.*, **216**, 214]

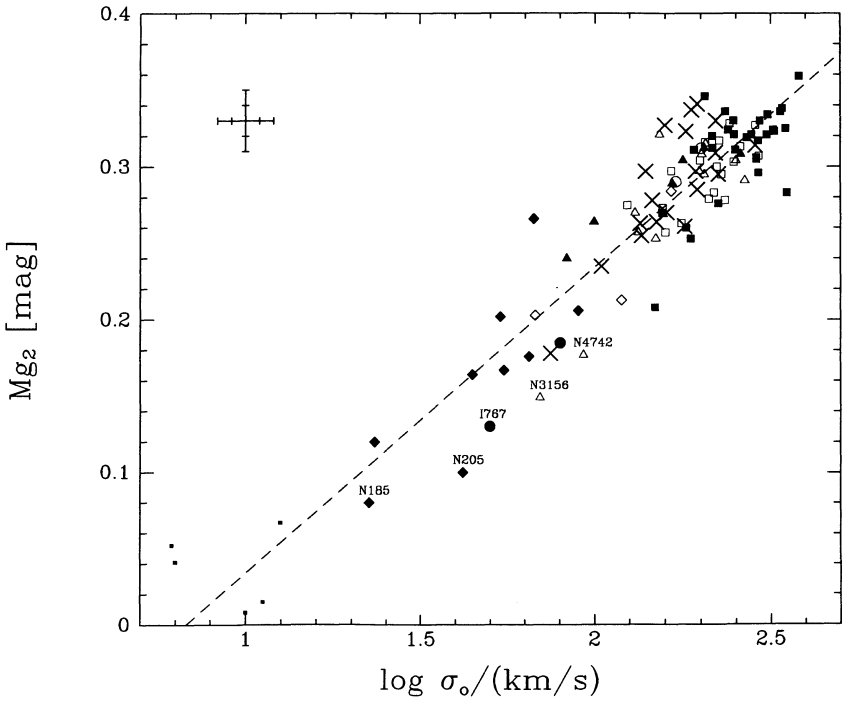

FIG. 3.—Nuclear Mg_2 index plotted against σ_0 for all types of DHGs (symbols coded as in Fig. 1). The dotted line represents the relation $Mg_2 = 0.20 \log \sigma_0 - 0.166$. Galaxies which show evidence for young or intermediate age stars are labeled. Representative error bars are shown in the upper left, the larger error bars refer to the objects with low values of σ_0, the smaller ones to luminous ellipticals and bulges. The Mg_2–log σ_0 correlation is tight over many decades in galaxy size and all DHG types.

[Bender, Burstein, & Faber 1993, *Ap.J.*, **411,** 153]

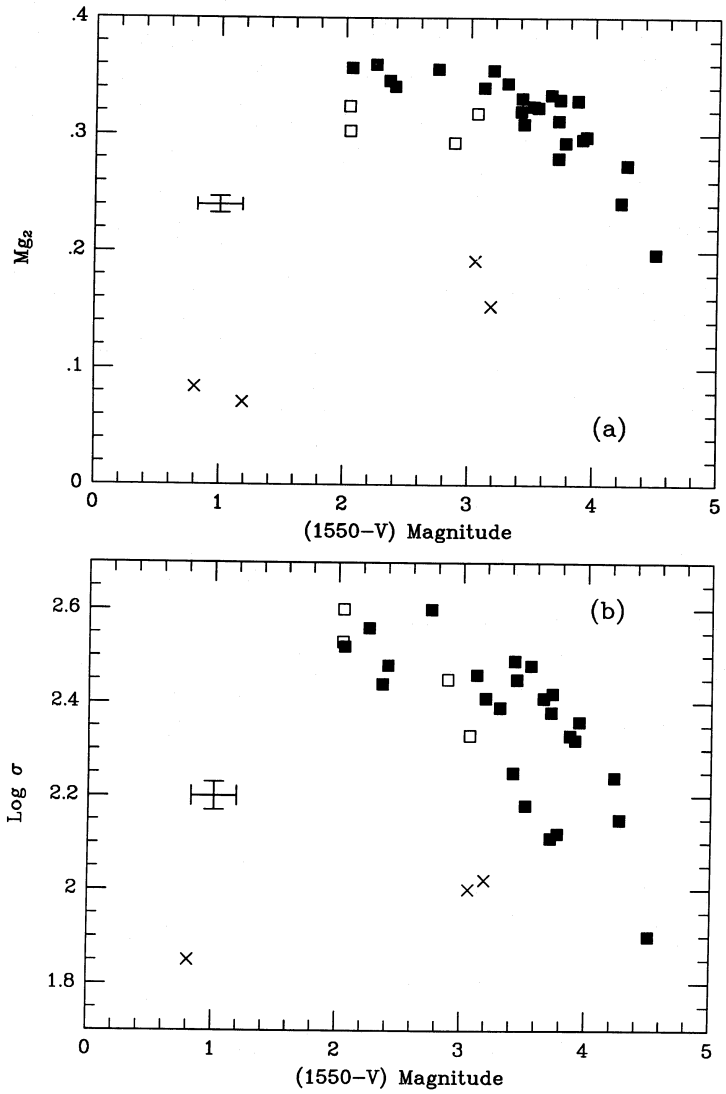

FIG. 1.—(*a*) The optical absorption-line index Mg_2 plotted vs. the ultraviolet/optical ($1550 - V$) color (expressed in magnitudes) for the 32 galaxies in this sample. Closed squares represent "quiescent" galaxies, open squares represent "active" galaxies, and crosses represent galaxies with on-going star formation. (*b*) Central velocity dispersions for 31 of the galaxies (NGC 205 excepted) vs. ($1550 - V$) color. Along with larger intrinsic scatter, there is no separation of active and quiescent galaxies in this plot.

[Burstein *et al.* 1988, *Ap.J.*, **328**, 440]

Elliptical Galaxy Surface Brightness Profiles

There are several ways to parameterize the observed luminosity profile of an elliptical galaxy. Let R be the projected radius of the galaxy, r be the true space, radius, $I(R)$ the observed surface brightness, and $j(r)$ the actual luminosity as a function of true space radius. (Remember, the light you see at a distance R is the sum of a line-of-sight through the galaxy.)

THE HUBBLE LAW

[Reynolds 1913, *MNRAS,* **74,** 132]
[Hubble 1930, *Ap.J.,* **71,** 231]

The original description of an elliptical galaxy's surface brightness was

$$I(R) = \frac{I_0}{(R/a+1)^2} \tag{6.06}$$

which, in terms of magnitudes, is

$$m(R) = m_0 + 5\log\left(\frac{R}{a}+1\right) \tag{6.07}$$

where a is the galaxy's characteristic radius. This law had the advantage that it was simple and, at large radii, it resembled an isothermal sphere. However, it implies a non-analytic form for the true space density, $j(r)$. Also, the total luminosity of the galaxy is

$$\begin{aligned}
\mathcal{L} &= \int_0^\infty 2\pi R \left\{ \frac{I_0}{((R/a)+1)^2} \right\} dR \\
&= 2\pi a^2 I_0 \int_0^\infty \frac{R}{(R+a)^2} dR \\
&= 2\pi a^2 I_0 \left\{ \ln(R+a) + \frac{a}{(R+a)} \right\} \Bigg|_0^\infty \\
&= \infty
\end{aligned} \tag{6.08}$$

THE DE VAUCOULEURS LAW

[de Vaucouleurs 1959, *Handbuch der Physik*]
[Young 1976, *A.J.*, **81,** 807]

The most famous description of an elliptical galaxy is the de Vaucouleurs $R^{1/4}$-law. According to the law, the surface brightness, in terms of magnitudes, is

$$m_R = a + bR^{1/4} \tag{6.09}$$

Most times, a and b are not quoted: instead, one parameterizes the galaxy in terms of its effective radius, R_e, and the surface brightness (in magnitudes per square arcsec) at R_e. R_e is defined as the observed radius which encloses half the galaxy's total light. To relate a and b to R_e and m_e, one starts with

$$m = a + bR^{1/4} \qquad m_e = a + bR_e^{1/4} \tag{6.10}$$

and differences these two equations

$$m - m_e = b\left\{R^{1/4} - R_e^{1/4}\right\} = bR_e^{1/4}\left\{(R/R_e)^{1/4} - 1\right\} \tag{6.11}$$

or

$$\log(I/I_e) = -\left(\frac{bR_e^{1/4}}{2.5}\right)\left\{(R/R_e)^{1/4} - 1\right\} \tag{6.12}$$

Since R_e by definition encloses half the light

$$\mathcal{L}(R_e) = \int_0^{R_e} 2\pi R \cdot I(R)dR = \int_0^{R_e} 2\pi R \cdot C \cdot 10^{-0.4(a+bR^{1/4})}dR \tag{6.13}$$

and

$$\begin{aligned}\frac{\mathcal{L}(R_e)}{\mathcal{L}_T} &= \int_0^{R_e} R \cdot e^{-0.4\ln(10)bR^{1/4}}dR \Bigg/ \int_0^{\infty} R \cdot e^{-0.4\ln(10)bR^{1/4}}dR \\ &= 0.5\end{aligned} \tag{6.14}$$

where C is the zero-point constant for the magnitude system. A (numerical) solution to this equation yields $bR_e^{1/4} = 8.327$. If one then substitutes this back into (6.12), one then gets the alternative form of the de Vaucouleurs law

$$\log\left(\frac{I}{I_e}\right) = -3.33071\left\{\left(\frac{R}{R_e}\right)^{1/4} - 1\right\} \tag{6.15}$$

where a and b are related to R_e and m_e via

$$R_e = \left(\frac{8.327}{b}\right)^4 \qquad m_e = a + 8.327 \tag{6.16}$$

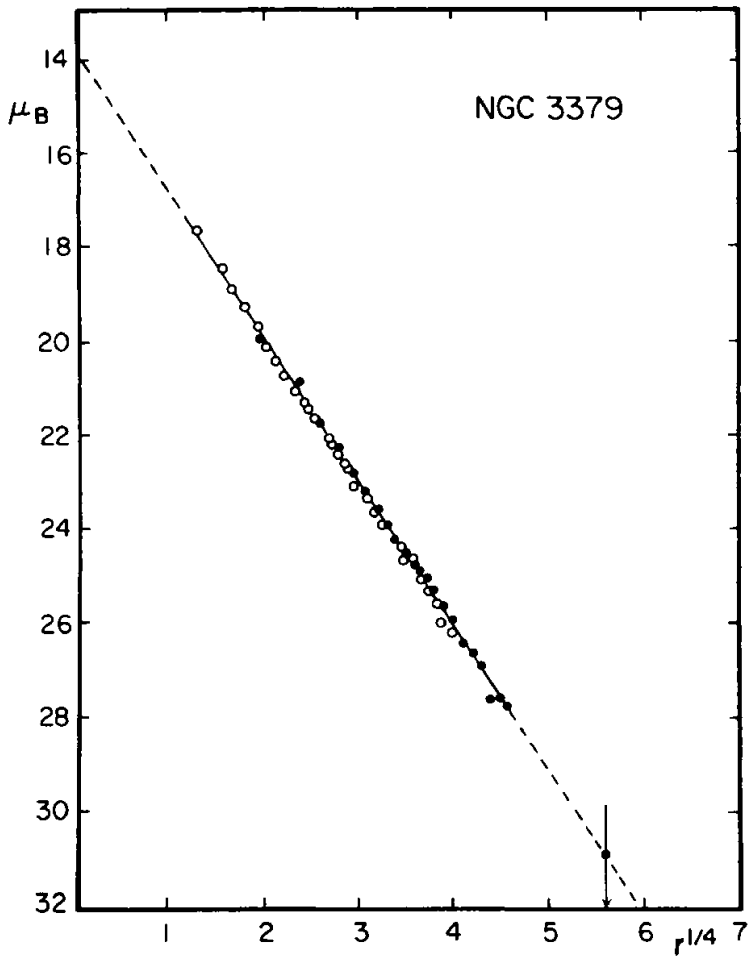

FIG. 2.—Mean E-W luminosity profile of NGC 3379 derived from McDonald photoelectric data. ●, Pe 4 data with 90 cm reflector; ○, Pe 1 data (M + P) with 2 m reflector. Note close agreement with $r^{1/4}$ law.

The advantages of the de Vaucouleurs law is that it is simple (in terms of magnitudes) and delivers a total galactic luminosity that is finite and reasonable. Specifically, the expression for total luminosity

$$\mathcal{L}_T = \int_0^\infty 2\pi R \cdot 10^{+0.4(C-a-bR^{1/4})} dR \tag{6.17}$$

has the form

$$\mathcal{L} \propto \int_0^\infty x^7 e^{-ax} dx \tag{6.18}$$

and the analytic solution

$$\mathcal{L}_T = 10^{-0.4(C-a)} \cdot \frac{\pi 8!}{(0.4 \ln(10) b)^8} \tag{6.19}$$

or

$$m_T = m_e - 3.388 - 5 \log R_e \tag{6.20}$$

The proof, which involves integrating by parts 7 times, is left to the ambitious student.

The disadvantages of the de Vaucouleurs law is that the space density (and galactic potential) implied by the law is non-analytic, so it is not convenient for modeling efforts.

THE JAFFE AND HERNQUIST LAWS

[Jaffe 1983, *MNRAS,* **202,** 995]
[Hernquist 1990, *Ap.J.,* **356,** 359]

There are two other laws that are used to model the luminosity profile of elliptical galaxies, the Jaffe law

$$j(r) = \frac{\mathcal{L} r_J}{4\pi r^2 (r + r_J)^2} \tag{6.21}$$

and the Hernquist model

$$j(r) = \frac{\mathcal{L}}{2\pi} \frac{a}{r(r+a)^3} \tag{6.22}$$

Note the different variables. The Hubble and de Vaucouleurs laws were observationally defined, hence R is the projected radius of the galaxy (observed on the sky) and I the observed surface brightness. For the Jaffe and Hernquist models, r is a 3-dimensional radius, and j is luminosity per unit volume (instead of per unit area). In the above equations, r_J and a are the free parameters that define the fit. For the Jaffe model, r_J is the space radius that contains half the light, and $R_e = 0.763\, r_J$; for the Hernquist model, a is the radius that contains one-quarter of the light, with $R_e = 1.8153\, a$. Both these laws have many useful analytic relations.

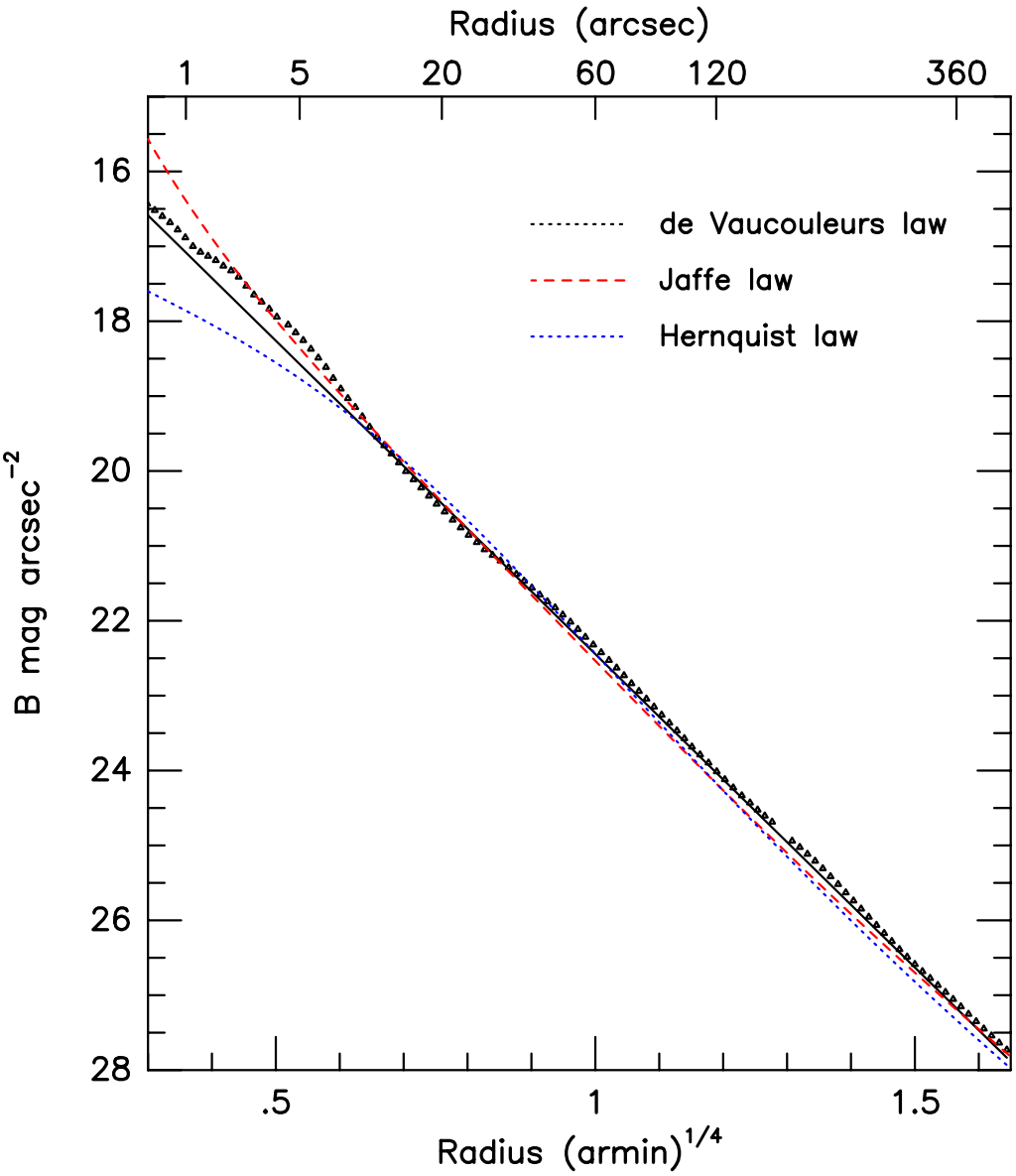

The de Vaucouleurs, Jaffe, and Hernquist surface brightness profiles of NGC 3379. The small triangles are the actual measurements of the galaxy.

THE JAFFE LAW

[Jaffe 1983, *MNRAS,* **202,** 995]

A useful relation, which has fallen out of favor over the best decade, is the Jaffe law for the true 3-D space density of an elliptical galaxy.

$$j(r) = \frac{\mathcal{L} r_J}{4\pi r^2 (r + r_J)^2} \tag{A.01}$$

where r_J is the Jaffe radius. This law has a number of advantages. First, it is simple. Second, it implies a total luminosity that is finite and easy to calculate

$$\begin{aligned} \mathcal{L}_T &= \int_0^\infty 4\pi r^2 j(r) dr \\ &= \int_0^\infty 4\pi r^2 \frac{\mathcal{L} r_J}{4\pi r^2 (r + r_J)^2} dr \\ &= \mathcal{L} r_J \int_0^\infty (r + r_J)^{-2} = \mathcal{L} r_J \, (r + r_J)^{-1} \Big|_0^\infty = \mathcal{L} \end{aligned} \tag{A.02}$$

The space radius containing 1/2 the light is also simple. From (A.02), the fraction of light contained in radius x is

$$f = \frac{\mathcal{L}(x)}{\mathcal{L}_T} = -\mathcal{L} r_J (r + r_J)^{-1} \Big|_0^x \Big/ - \mathcal{L} r_J (r + r_J)^{-1} \Big|_0^\infty \tag{A.03}$$

For $f = 0.5$, this is easily solved: $x = r_J$. The Jaffe radius is therefore the radius within the galaxy that contains half the light. For reference, r_J is related to the galaxy's effective radius (*i.e.,* the projected radius which encloses half the light) by $r_J = 1.3106 \, R_e$.

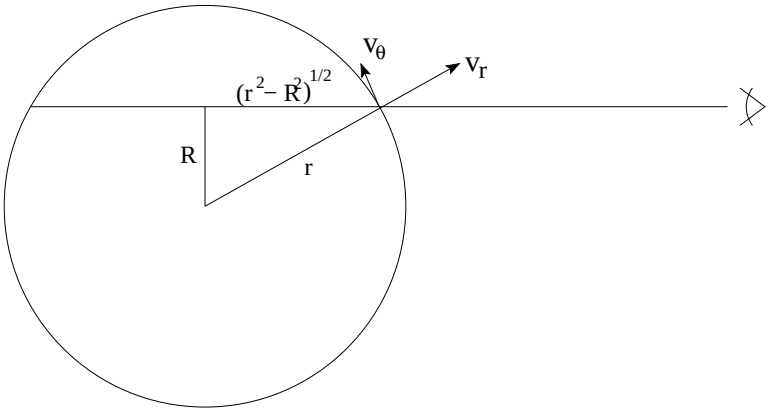

To go from true space density to projected density, one must integrate along the line-of-sight, z

$$I(R) = \int_R^\infty j(r)dz = 2\int_R^\infty j(r) \cdot \frac{r}{\left(r^2 - R^2\right)^{1/2}}\, dr \qquad \text{(A.04)}$$

which, for the Jaffe law, is

$$I(R) = \frac{2\mathcal{L}r_J}{2\pi}\int_R^\infty \frac{1}{r^2(r+r_J)^2} \cdot \frac{r}{\left(r^2 - R^2\right)^{1/2}}\, dr \qquad \text{(A.05)}$$

This integral is analytic, though its solution is long

$$I(R) = \frac{\mathcal{L}}{r_J^2}\left\{\frac{r_J}{4R} + \frac{1}{2\pi}\left[\frac{r_J^2}{r_J^2 - R^2} - \frac{2r_J^3 - r_J R^2}{\left(r_J^2 - R^2\right)^{3/2}}\text{arccosh}\left(\frac{r_J}{R}\right)\right]\right\} \qquad \text{(A.06)}$$

for $R < r_J$, and

$$I(R) = \frac{\mathcal{L}}{r_J^2}\left\{\frac{r_J}{4R} + \frac{1}{2\pi}\left[\frac{r_J^2}{R^2 - r_J^2} + \frac{r_J R^2 - 2r_J^3}{\left(R^2 - r_J^2\right)^{3/2}}\arccos\left(\frac{r_J}{R}\right)\right]\right\} \qquad \text{(A.07)}$$

for $R > r_J$.

While the above properties of the Jaffe law are interesting, the true purpose of the expression is for galactic dynamics. For the case of a constant mass-to-light ratio (Υ), the law yields a simple, analytic expression for the galactic potential. If one converts luminosity to mass via $\mathcal{M} = \Upsilon\mathcal{L}$, then the space density of matter in a Jaffe elliptical is law

$$\rho(r) = \frac{\mathcal{M} r_J}{4\pi r^2 \left(r + r_J\right)^2} \tag{A.08}$$

One can plug this into Poisson's equation

$$\frac{1}{r^2}\frac{d}{dr}\left(r^2 \frac{d\Phi}{dr}\right) = 4\pi G\rho \tag{A.09}$$

to get

$$\frac{d}{dr}\left(r^2 \frac{d\Phi}{dr}\right) = \frac{4\pi G\mathcal{M} r_J r^2}{4\pi r^2 (r + r_J)^2} = \frac{G\mathcal{M} r_J}{\left(r + r_J\right)^2} \tag{A.10}$$

This can easily be integrated to yield

$$r^2 \frac{d\Phi}{dr} = G\mathcal{M} r_J \int \frac{dr}{\left(r + r_J\right)^2} = -\frac{G\mathcal{M} r_J}{(r + r_J)} + C \tag{A.11}$$

where C is the constant of integration. Since the force at $r = 0$ must be identically zero,

$$\frac{d\Phi}{dr}(r = 0) = -\frac{G\mathcal{M}}{r^2}\left(\frac{r_J}{r + r_J}\right) + \frac{C}{r^2} = 0 \Longrightarrow C = G\mathcal{M} \tag{A.12}$$

Thus, the potential implied by the Jaffe law is

$$\begin{aligned}\Phi &= \int -\frac{G\mathcal{M}r_J}{r^2\,(r+r_J)} + \frac{G\mathcal{M}}{r^2}\,dr \\ &= \int -\frac{G\mathcal{M}r_J}{r^2\,(r+r_J)} + \frac{G\mathcal{M}(r+r_J)}{r^2(r+r_J)}\,dr \\ &= \int \frac{G\mathcal{M}}{r(r+r_J)}\,dr \\ &= \frac{G\mathcal{M}}{r_J}\ln\left(\frac{r}{r+r_J}\right) \end{aligned} \tag{A.13}$$

Finally, for the case of purely isotropic or circular orbits, the Jaffe law yields expressions for the stellar velocity dispersions that are analytic. From galactic dynamics, the Jeans equation in spherical coordinates is

$$\frac{\partial\rho\langle v_r^2\rangle}{\partial r} + \frac{\rho}{r}\left\{2\langle v_r^2\rangle - \left(\langle v_\theta^2\rangle + \langle v_\phi^2\rangle\right)\right\} = -\rho\,\frac{\partial\Phi}{\partial r} \tag{A.14}$$

where $\langle v_r^2\rangle$, $\langle v_\theta^2\rangle$, and $\langle v_\phi^2\rangle$ are the radial, tangential, and azimuthal stellar velocity dispersions. To simplify the notation, we define the radial and tangential "pressures" as density-weighted velocity dispersions, *i.e.,*

$$P = \rho\,\langle v_r^2\rangle \qquad Q = \rho\left(\langle v_\theta^2 + \langle v_\phi^2\rangle\right) \tag{A.15}$$

so the Jeans equation is

$$\frac{dP}{dr} + \frac{(2P-Q)}{r} = -\rho\frac{d\Phi}{dr} \tag{A.16}$$

If we substitute in the densities and force law implied by the Jaffe model

$$\frac{dP}{dr} + \frac{(2P - Q)}{r} = -\frac{\mathcal{M} r_J}{4\pi r^2 (r + r_J)^2} \cdot \frac{G\mathcal{M}}{r_J} \frac{r}{r + r_J} \cdot \left\{ \frac{1}{r + r_J} - \frac{r}{(r + r_J)^2} \right\}$$

$$= -\frac{G\mathcal{M}^2 \, r_J}{4\pi r^3 \, (r + r_J)^3} \tag{A.17}$$

This is a relatively simple expression, which reduces further in the presence of isotropic or circular orbits. In the isotropic case, $\langle v_r^2 \rangle = \langle v_\theta^2 \rangle = \langle v_\phi^2 \rangle$, so $P = Q/2$, and the Jeans equation becomes

$$\frac{dP}{dr} = -\frac{G\mathcal{M}^2 \, r_J}{4\pi r^3 \, (r + r_J)^3} \tag{A.18}$$

which has the solution

$$P = -\frac{G\mathcal{M}^2 \, r_J}{4\pi} \int r^{-3} \, (r + r_J)^{-3} \, dr$$

$$= \frac{G\mathcal{M}^2 r_J}{4\pi r^2 (r + r_J)^2} \cdot \left\{ \frac{r_J^3 - 2r_J^2 r - 18 r_J r^2 - 12 r^3}{2 r_J^4} - \frac{6 r^2 (r + r_J)^2}{r_J^5} \ln\left(\frac{r}{r + r_J} \right) \right\} \tag{A.19}$$

or, since $\langle v_r^2 \rangle = P/\rho$,

$$\langle v_r^2 \rangle = \frac{G\mathcal{M}}{2 r_J^4} \cdot \left\{ r_J^3 - 2 r_J^2 r - 18 r_J r^2 - 12 r^3 - \frac{12 r^2 (r + r_J)^2}{r_J} \ln\left(\frac{r}{r + r_J} \right) \right\} \tag{A.20}$$

For circular orbits, $\langle v_r^2 \rangle = 0$, so $P = 0$, and the solution is even easier

$$\frac{dP}{dr} + \frac{(2P - Q)}{r} = -\frac{Q}{r} = -\rho \frac{d\Phi}{dr} = -\frac{G\mathcal{M}^2\, r_J}{4\pi} \cdot \frac{1}{r^3 (r + r_J)^3} \tag{A.21}$$

which implies

$$Q = \frac{G\mathcal{M}^2\, r_J}{4\pi r^2 (r + r_J)^3} \tag{A.22}$$

and

$$\langle v_\theta^2 \rangle = \langle v_\phi^2 \rangle = \frac{G\mathcal{M}}{r + r_J} \tag{A.23}$$

Note that this means that the circular velocity at any point is just

$$v_c = \left(\frac{G\mathcal{M}}{r + r_J} \right)^{1/2} \tag{A.24}$$

The law also implies a finite velocity dispersion at $r = 0$.

The only disadvantages of the Jaffe law is that the implied phase-space stellar distribution function is complicated (involving things called Dawson integrals), and the density and potential at $r = 0$ is infinite. However, even at $r = 0$, the total enclosed light of the Jaffe law is finite.

THE HERNQUIST LAW

[Hernquist 1990, *Ap.J.*, **356,** 359]

Today, the model that is most used for elliptical galaxies (and some groups and clusters) is the Hernquist law

$$j(r) = \frac{\mathcal{L}}{2\pi} \cdot \frac{a}{r(r+a)^3} \tag{A.25}$$

It has many of the same advantages as the Jaffe model. It is a simple law that implies a finite total luminosity

$$\begin{aligned} \mathcal{L}_T &= \int_0^\infty 4\pi r^2 j(r)\, dr \\ &= \int_0^\infty \frac{2\mathcal{L}ar}{(r+a)^3}\, dr \\ &= 2\mathcal{L}a \left\{ \frac{a}{2(r+a)^2} - \frac{1}{r+a} \right\} \Bigg|_0^\infty = \mathcal{L} \end{aligned} \tag{A.26}$$

Like r_J, a is a scale factor: the space density that contains 1/4 of the total light. For comparison, the half-light space radius $r_{1/2} = (1+\sqrt{2})a$, and the effective radius is $R_e = 1.8153\, a$. Also, like the Jaffe law, the Hernquist model has a messy, but analytic form for the surface brightness

$$\begin{aligned} I(R) &= 2\int_R^\infty j(r) \cdot \frac{r}{(r^2-R^2)^{1/2}}\, dr \\ &= 2\int_0^\infty \frac{\mathcal{L}a}{2\pi} \cdot \frac{r}{r(r+a)^3(r^2-R^2)^{1/2}}\, dr \\ &= \frac{\mathcal{L}}{2\pi a^2(1-s^2)^2} \cdot \left\{ (2+s^2)\chi(s) - 3 \right\} \end{aligned} \tag{A.27}$$

where $s = R/a$, and

$$\chi(s) = \frac{1}{\sqrt{1-s^2}} \ \text{sech}^{-1}\, s \quad \text{for} \quad 0 \le s \le 1$$

$$= \frac{1}{\sqrt{s^2-1}} \ \sec^{-1} s \quad \text{for} \quad 1 \le s \le \infty \tag{A.28}$$

If the mass-to-light ratio is constant, the Hernquist model's expression for the potential is simple and analytic. When the density profile

$$\rho(r) = \frac{\mathcal{M}}{2\pi} \cdot \frac{a}{r(r+a)^3} \tag{A.29}$$

is substituted into Poisson's equation

$$\frac{1}{r^2}\frac{d}{dr}\left(r^2 \frac{d\Phi}{dr}\right) = 4\pi G \cdot \frac{\mathcal{M}}{2\pi} \cdot \frac{1}{r(r+a)^3} \tag{A.30}$$

then

$$\frac{d\Phi}{dr} = \frac{2G\mathcal{M}a}{r^2} \int \frac{r}{(r+a)^3}\, dr$$

$$= \frac{2G\mathcal{M}a}{r^2} \left\{ -\frac{2r+a}{2(r+a)^2} + C \right\} \tag{A.31}$$

Since the force must equal zero at $r = 0$,

$$C = \frac{2r+a}{2(r+a)^2} = \frac{1}{2a} \tag{A.32}$$

and

$$\Phi = 2G\mathcal{M}a \int -\frac{2r+a}{2r^2(r+a)^2} + \frac{1}{2ar^2}\, dr$$

$$= 2G\mathcal{M}a \int \frac{1}{2a(r+a)^2}\, dr$$

$$= -\frac{G\mathcal{M}}{r+a} \tag{A.33}$$

Also like the Jaffe law, the Hernquist law yields analytic expressions for the radial and tangential pressures in the case of isotropic and circular orbits.

$$\begin{aligned}\frac{dP}{dr} + \frac{(2P-Q)}{r} &= -\rho\,\frac{d\Phi}{dr} \\ &= \frac{\mathcal{M}}{2\pi}\cdot\frac{a}{r(r+a)^3}\cdot\frac{G\mathcal{M}}{(r+a)^2} \\ &= -\frac{G\mathcal{M}^2 a}{2\pi}\frac{1}{r(r+a)^5}\end{aligned} \tag{A.34}$$

For isotropic orbits where $Q = 2P$,

$$\begin{aligned}P &= -\frac{G\mathcal{M}^2 a}{2\pi}\int r^{-1}(r+a)^{-5}dr \\ &= \frac{G\mathcal{M}^2}{24\pi(r+a)^4}\cdot\left\{\frac{12(r+a)^4}{a^4}\ln\left(\frac{r+a}{a}\right) - 25\right. \\ &\qquad \left. - 52\left(\frac{r}{a}\right) - 42\left(\frac{r}{a}\right)^2 - 12\left(\frac{r}{a}\right)^3\right\}\end{aligned} \tag{A.35}$$

and

$$\begin{aligned}\langle v_r^2\rangle = \frac{G\mathcal{M}}{12(r+a)}\left(\frac{r}{a}\right)\cdot\left\{\frac{12(r+a)^4}{a^4}\ln\left(\frac{r+a}{a}\right) - 25\right. \\ \left. - 52\left(\frac{r}{a}\right) - 42\left(\frac{r}{a}\right)^2 - 12\left(\frac{r}{a}\right)^3\right\}\end{aligned} \tag{A.36}$$

For circular orbits

$$Q = \frac{G\mathcal{M}^2 a}{2\pi(r+a)^5} \tag{A.37}$$

and

$$\langle v_\theta^2 \rangle = \langle v_{\rm circ}^2 \rangle = Q/\rho = \frac{G\mathcal{M} r}{(r+a)^2} \tag{A.38}$$

Finally, and perhaps most remarkably, in the case of isotropic and circular orbits, the expressions for σ_p^2, the *observed* velocity dispersion (which is the sum of the stellar motions all along the line-of-sight), is analytic. In general, this intensity-weighted measurement is given by

$$I(R)\sigma_p^2(R) = 2\int_R^\infty \left(1 - \beta\,\frac{R^2}{r^2}\right) P\,\frac{r}{(r^2-R^2)^{1/2}}\,dr \tag{A.39}$$

where β describes the degree of orbital anisotropy

$$\beta = 1 - \frac{\langle v_\theta^2 \rangle}{\langle v_r^2 \rangle} \tag{A.40}$$

For isotropic orbits, $\beta = 0$, and after *a lot* of math,

$$\begin{aligned}\sigma_p^2(R) = \frac{G\mathcal{M}^2}{12\pi a^3 I(R)} \cdot \Bigg\{ & \frac{1}{2}\frac{1}{(1-s^2)^3} \cdot \\ & \Big[-3s^2\chi(s)\left(8s^6 - 28s^4 + 35s^2 - 20\right) \\ & -24s^6 + 68s^4 - 65s^2 + 6\Big] - 6\pi s \Bigg\}\end{aligned} \tag{A.41}$$

For circular orbits, $\beta = -\infty$, and

$$\sigma_p^2(R) = \frac{G\mathcal{M}^2 R^2}{2\pi a^5 I(R)} \cdot \left\{ \frac{1}{24(1-s^2)^4} \cdot \right.$$
$$\Big[-\chi(s)\left(24s^8 - 108s^6 + 189s^4 - 120s^2 + 120\right)$$
$$\left. - 24s^6 + 92s^4 - 117s^2 + 154\Big] + \frac{\pi}{2s} \right\} \qquad \text{(A.42)}$$

Like the Jaffe law, the Hernquist model has an analytic, though complicated, expression for the stellar density in phase space, and possesses an infinite density at its center. The enclosed luminosity, however, is finite throughout.

$$\mathcal{L} = \int_0^r 4\pi r^2 \cdot \frac{\mathcal{L}}{2\pi} \cdot \frac{a}{r(r+a)^3}\, dr = \int_0^r \frac{2\mathcal{L}ar}{(r+a)^3}\, dr$$
$$= 2\mathcal{L}a \left\{ \frac{a}{2(r+a)^2} - \frac{1}{(r+a)} \right\} \qquad \text{(A.43)}$$

Unlike the Jaffe law, the radial velocity dispersion at the center of a Hernquist model galaxy is $\langle v_r^2 \rangle = 0$. (But this is not necessarily a bad thing.)